Journal of Fluids and Structures (2001) **15,** 503–512
doi:10.1006/jfls.2000.0364, available online at http://www.idealibrary.com on IDEAL®

GALLOPING RESPONSE OF A CYLINDER WITH UPSTREAM WAKE INTERFERENCE

F. S. Hover and M. S. Triantafyllou

Department of Ocean Engineering, Massachusetts Institute of Technology
77 Massachusetts Avenue, Cambridge, MA 02139, U.S.A.

(Received 3 September 2000, and in final form 15 November 2000)

A compliantly-mounted rigid cylinder was towed at $\mathrm{Re} = 3 \times 10^4$, 4·75 diameters behind a stationary leading cylinder of the same size. An in-line configuration and a 12-degree staggered arrangement each produced large-amplitude galloping responses, and an upward extension of the frequency lock-in range to a reduced velocity of at least 17. The frequency lock-in begins at nearly the same free-stream reduced velocity as a single cylinder, while a large phase change in the lift force occurs at higher reduced velocities, which can be extrapolated from the single-cylinder lock-in point. Force spectra indicate that shedding from the upstream cylinder is completely unaffected by motions of the trailing cylinder. Furthermore, the motion-coupled peaks suggest that only one lift force cycle and one or two drag force cycles occur per oscillation, the latter depending on the offset.

1. INTRODUCTION

The wake interaction of parallel cylinders arises in many applications, including arrays of offshore risers and moorings, and power transmission lines. For nonoscillating cylinders, a number of distinct flow regimes exist, which depend on the separation distance S (Zdravkovich & Pridden 1977; Igarashi 1981). Small separation distances ($S/D < 2$) limit the reattachment of the leading cylinder's shear layer to the trailing one, and can lead to bistable gap flows. Quasi-steady recirculation cells, with coupled vortex formation, occur for larger separation distances ($2 < S/D < 4$), and, finally, vortex roll-up from the leading cylinder occurs for $S/D > 4$, where coupling is diminished. For the case of forced vibrations of two tandem cylinders, a wake lock-in exists for the extreme motion phase angles of zero and 180°, and lock-in of the wake to the motion occurs over a dramatically expanded region of amplitude and frequency, for small S (Mahir & Rockwell 1996).

In tests where both cylinders are compliantly-mounted, large-amplitude vibrations of both cylinders can occur when the separation is about 5–7D, and at least for lateral offsets up to 1·5D (Zdravkovich 1985). The vibrations are limited to a specific range of reduced velocities, typically beginning at lower values than for a single cylinder.

Bokaian & Geoola (1984) considered the case of a fixed leading cylinder, and a compliantly-mounted trailing cylinder. They report both vortex-resonance regions, i.e., motion occurring only over a specific range of reduced velocity, and galloping instabilities, where motions persist for high reduced velocities. These two types of responses can occur independently or coalesce, depending on the separation distance. Vortex resonance occurs alone for $S/D > 3$, for both the in-line case and with offsets of one diameter. In other tests at much higher Reynolds number, galloping is suggested for $S/D < 7$, diminishing as the vortex-induced vibration is recovered for large S/D (Brika & Laneville 1999).

0889–9746/01/040503 + 10 $35.00/0

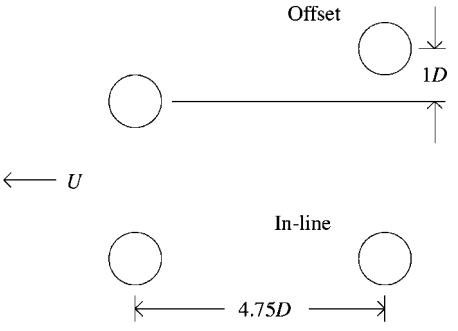

Figure 1. Configurations for the in-line and offset VIV tests.

The tandem arrangement of two cylinders in mid-proximity ($S/D = 5$–10) creates a reduced natural shedding frequency, with comparison to a single cylinder. When one cylinder vibrates freely, however, the wake frequency behind the leading cylinder is unaffected by the trailing cylinder. The wake of the trailing cylinder still exhibits a lower Strouhal frequency, consistent with reduced mean flow calculations, until it reaches lock-in conditions. Hence, on a reduced-velocity scale employing free-stream velocity, frequency lock-in occurs at a higher value than for a single cylinder (Brika & Laneville 1999).

In order to bridge some of these results, we consider here a compliantly-mounted rigid circular cylinder in the wake of a stationary fixed cylinder of the same diameter. Locations for the trailing cylinder are 4·75 diameters downstream (tandem), and 4·75 diameters downstream, with a lateral offset of one diameter (relative angle 12°); see Figure 1. These locations are near Zdravkovich's point of maximum response, and near the edge of the wake interference zone, respectively.

2. APPARATUS AND EXPERIMENTAL SETUP

Tests were conducted at the MIT Testing Tank facility, a $30 \times 2{\cdot}5 \times 1{\cdot}2$ m still-water towing tank. We used rigid aluminum cylinders with diameter $D = 7{\cdot}62$ cm and span $L = 200$ cm, moving at constant speed horizontally; the downstream cylinder oscillates transversely to the flow (in the vertical direction). A view of the device from inside the tank is given in Figure 2. The cylinders terminate with 0·2 cm gaps onto 31 cm diameter end-plates at each end. The downstream cylinder is supported by a pair of three-axis piezoelectric load cells, which in turn attach to a heaving structure that also supports the end-plates. This assembly is positioned using a lead screw with 30 cm travel, driven by a brushless servomotor. The uniform tow velocity for the tests corresponds with $\mathrm{Re} = 3{\cdot}05 \times 10^4$.

We employed a robotic force-feedback loop as described in Hover *et al.* (1998). In this system, dynamic lift force measurements are injected into a real-time simulation of a compliant structure, whose output drives the servomotor reference trajectory, and ultimately the physical cylinder. The functional result is a cylinder that appears to be compliantly mounted, even though its position is controlled very accurately with a servomotor. In the present experiments, the simulated compliance consisted of a simple mass and spring. The simulation mass M and stiffness K can be arbitrarily specified by the user, thus allowing the variation of nominal reduced velocity $V_{rn} = 2\pi U/\omega_n D$ at constant Reynolds number. Here, U represents the steady towing speed of the carriage, and $\omega_n = \sqrt{K/M}$ is the undamped natural frequency of the virtual structure.

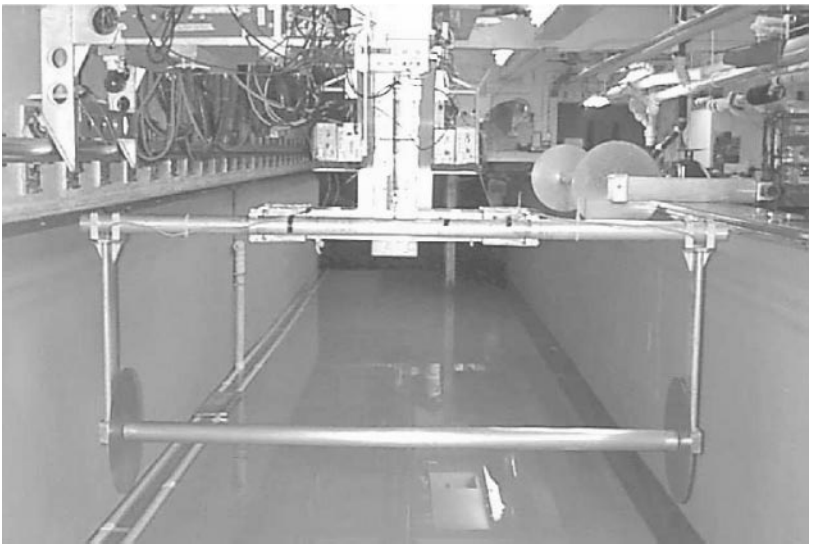

Figure 2. The testing apparatus installed at the MIT Towing Tank, showing one 2 m cylinder, with end-plates and lower yoke assembly. Photo viewpoint is inside the tank.

Intrinsic in the feedback loop is a correction for the component of measured force that is due to the inertia in the material test cylinder; this mass is effectively replaced with M. The data in the current work were obtained with the nondimensional mass ratio $m^* = 4M/\rho\pi D^2 L = 3{\cdot}0$, and an effective damping ratio of about 4%. The nonzero damping ratio is an artifact of the closed-loop control system, which imposes some phase loss to achieve smooth operation.

The following coefficients are calculated for each test: (i) average 1/10th-highest amplitude/diameter ratio $A/D_{1/10}$, with excursions taken from the mean position; (ii) mean drag coefficient, mean(C_d); (iii) fluctuating drag coefficient std(C_d), the standard deviation of the drag signal; (iv) total lift coefficient amplitude $C_l = 2|F|/\rho DLU^2$, constructed as the Euclidean norm of components in phase with vibration velocity and position; (v) phase angle ϕ, between the oscillating lift force and the imposed motion, computed as an arctangent of the lift coefficients in phase with velocity and position.

3. AMPLITUDE, DRAG, AND LIFT COEFFICIENTS

We give the amplitudes and force coefficients in Figure 3, and the phase angle in Figure 4. In each figure, the calculated value is plotted against nominal reduced velocity for three configurations: (a) in-line, (b) offset, and (c) single cylinder.

The case of a single cylinder is provided for comparison with previously published results, and reflects a number of typical characteristics. First, as V_{rn} increases, the amplitude ratio approaches unity, then drops to a short plateau with $A/D \approx 0{\cdot}75$, and then a longer plateau at $A/D \approx 0{\cdot}50$, before dropping again in the range of $V_{rn} = 9$–11. This type of A/D response envelope, i.e. localized on the V_{rn}-axis, is termed vortex resonance in the sequel. The highest-amplitude part of the curve correlates with a steady drag coefficient of about 3·0, and the main plateau matches the zero-motion drag coefficient of 1·25. A similar dependence can be observed for the fluctuating component of drag, as well as lift coefficient magnitude.

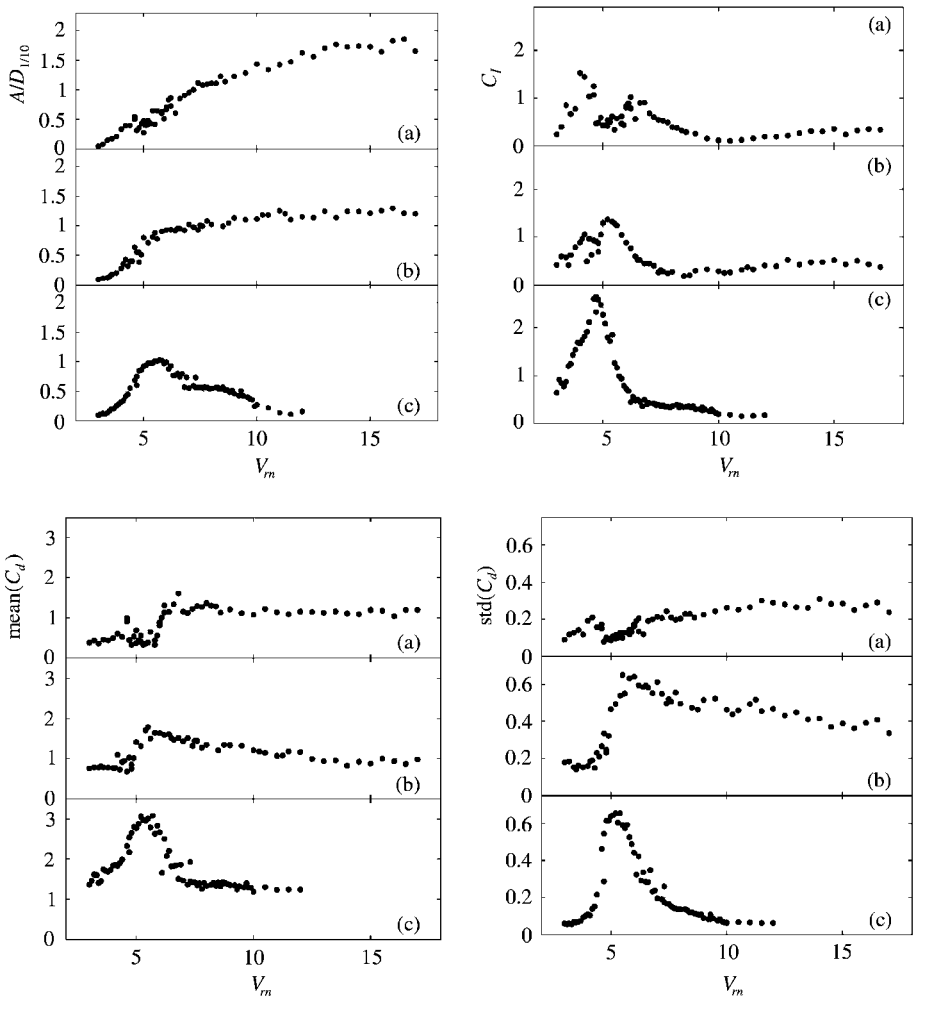

Figure 3. Average one-tenth highest amplitude of motion (upper left), mean drag coefficient (lower left), fluctuating lift coefficient (upper right), and fluctuating drag coefficient (lower right), as functions of V_{rn}: (a) in-line; (b) offset; (c) single cylinder.

The phase angle for the single cylinder in free-vibration undergoes a rapid transition from near zero to near 180°, near $V_{rn} = 6{\cdot}0$; this event generally marks a mode change from "2S" - to "2P"-type vortex shedding, evident in forced and free vibrations (Williamson & Roshko 1988; Brika & Laneville 1993). The phase points near 90°, amid the transition, result from averaging the phase calculated at each end of the cylinder. In this regime, we often observe one large-amplitude end force with 0° phasing, and one small-amplitude end force with 180° phasing.

For both configurations involving interference, galloping occurs, without any clear signatures of vortex resonance; the growth of motion with V_{rn} is largely monotonic. Amplitude ratios become very high, reaching 1·9 in the in-line case and 1·3 in the offset case. It is likely that larger amplitudes could also occur at higher velocities.

Steady drag coefficients for the in-line and offset cases with no vibration, i.e. low V_{rn}, are 0·35 and 0·80, respectively. These values are in reasonable agreement with Zdravkovich

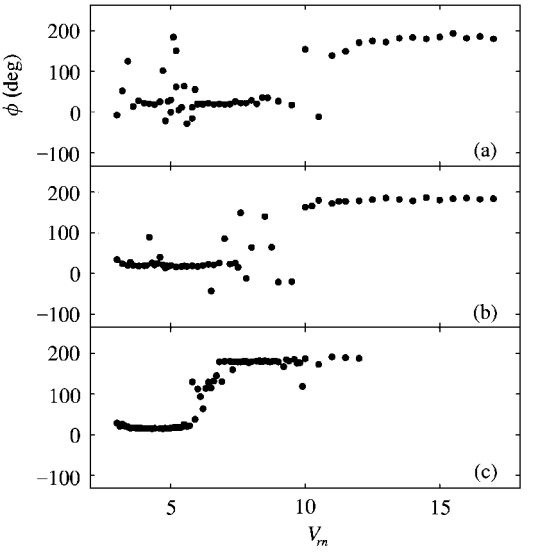

Figure 4. Lift coefficient phase ϕ as a function of V_{rn}: (a) in-line; (b) offset; (c) single cylinder.

& Pridden (1977), and also with the mean wake analysis described by Huse (1992), for which trailing cylinder C_d values of 0·49 and 0·83 are generated from a base C_d of 1·2. For the in-line case, the mean drag jumps from 0·35 to about 1·2, at $V_{rn} \approx 6$, although some scatter exists. In contrast, the offset case has C_d increasing to about 1·8 at $V_{rn} \simeq 5$, before a gradual descent to about 1·0 at the higher V_{rn}. Roughly speaking, these upward jumps in mean C_d for both configurations correspond to regimes of highly irregular amplitude ratios.

Fluctuating drag for the offset case reaches the same maximum value as the single cylinder, although at a slightly higher V_{rn}, and then declines gradually to a value near 0·4, markedly higher than the single cylinder. When the trailing cylinder is in-line, values are much lower overall, and a local minimum at $V_{rn} \approx 5{\cdot}5$ is in the same area of scattered amplitudes noted above.

Peak lift coefficients C_l for the interference cases are much lower than for the single cylinder, and both curves have an area of low value, again roughly in the regime of scattered amplitudes. Noteworthy is the fact that each lift coefficient has the nature of a vortex resonance, in the sense that it decays at high velocities. Phase angle, however, indicates that the main transition occurs well away from the usual range of V_{rn}. The in-line configuration changes phase at $V_{rn} = 9$–11, while it changes over a larger range, $V_{rn} = 7$–10, for the offset case. Several effects are likely. The in-line cylinder arrangement imposes a reduced mean flow on the trailing cylinder, while in the offset case, the trailing cylinder can additionally emerge from the wake periodically, and is therefore exposed to higher velocities. Further discussion of phase variation is given in Section 5.

Interestingly, no unique features in any of the other coefficient plots (Figure 3) signal the phase change with wake interference. For the single cylinder, amplitude and mean drag both drop dramatically through the phase change.

4. SPECTRAL DESCRIPTION OF RESPONSES

In Figures 5–7 are plotted the spectral content of the displacement, and lift and drag forces. Each set of Fourier transform magnitudes has arbitrary scaling, and these are overlaid on

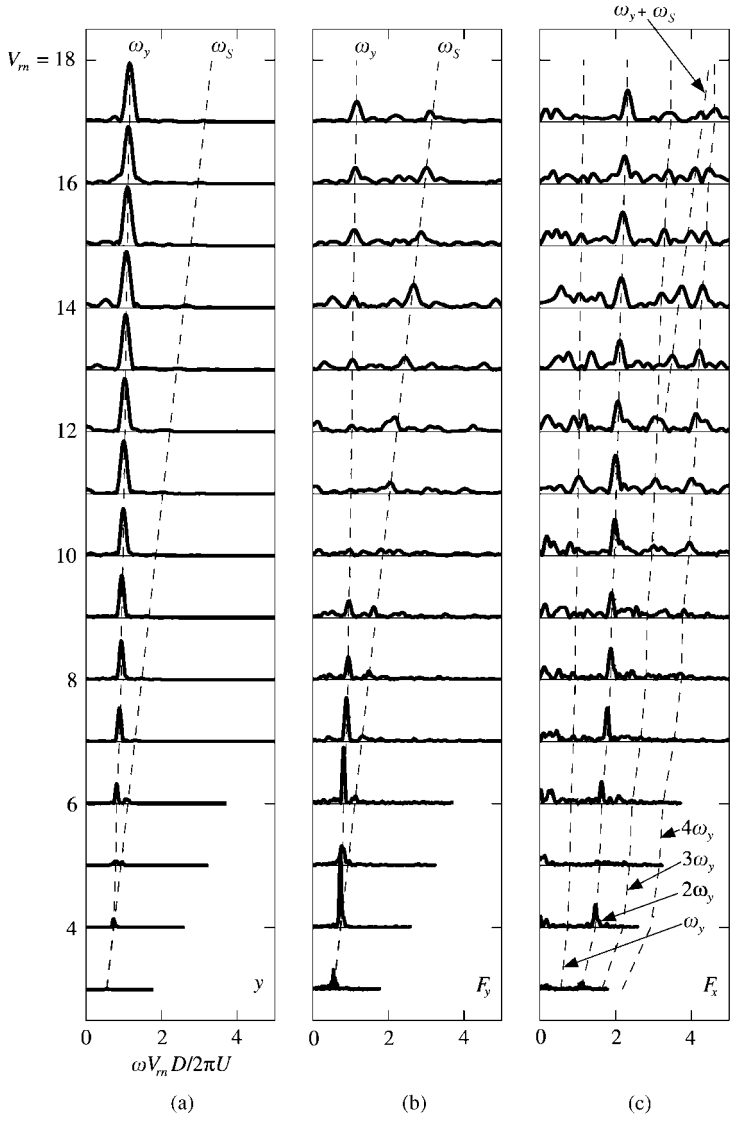

Figure 5. (a) Displacement and (b, c) force spectra of a cylinder centered 4·75D behind a stationary leading cylinder.

a vertical V_{rn}-axis. The horizontal axis carries normalized frequency, scaled so that unity corresponds with the undamped natural frequency of the structure. Dashed lines are also given in each subplot, which follow the evolution of various peaks. Spectral peaks widen at the higher reduced velocities, but this is only a remnant of the frequency nondimensionalization, since all of the tests were performed at the same physical velocity.

In Figure 7 (single cylinder), the lines classify features in the following ways. The displacement (y) and lift (F_y) peaks follow the single-cylinder shedding frequency ω_S (St = 0·185) at low V_{rn}, and lock on to the structural mode ω_n at around $V_{rn} = 6{\cdot}5$. The locked-in nondimensional frequency $\omega_y/\omega_n \simeq 1{\cdot}15$ is typical for tests with $m^* = 3$, where negative added mass significantly increases the net natural frequency. Lift force spectra track the motion spectra closely, becoming quite small for $V_{rn} > 10$. The fluctuating drag

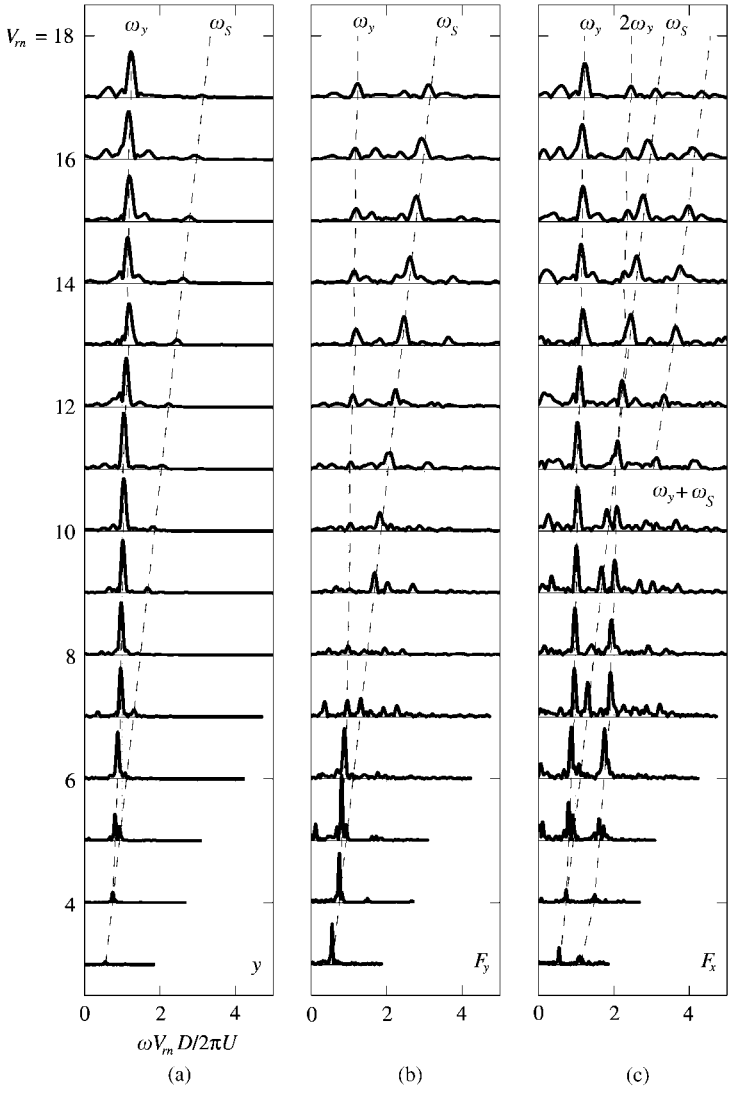

Figure 6. (a) Displacement and (b, c) force spectra of a cylinder located 4·75D behind a stationary leading cylinder, with a one-diameter lateral offset.

force (F_x) is significant only near the onset of lock-in, and the peak here follows the second harmonic of ω_y. The lift and drag forces thus indicate the simplest modes of VIV, involving 2S and 2P types of wake.

For the in-line experiments of Figure 5, oscillations are narrow-banded, and occur near and just above ω_n; the amplitude $A/D_{1/10}$ grows throughout the range of reduced velocity. Lift has very significant components at both the frequency of motion ω_y and at ω_S, especially for high V_{rn}. The shedding frequency plotted here is the *same* as that for the single cylinder, and therefore likely relates to the incoming wake. Below the phase change at $V_{rn} \simeq 10$, the lift force is primarily at ω_y; above the phase change, ω_S dominates for a short while, before a peak at ω_y grows to similar magnitude. The phase transition occurs at a V_{rn} where the lift force peaks are broad-banded and small.

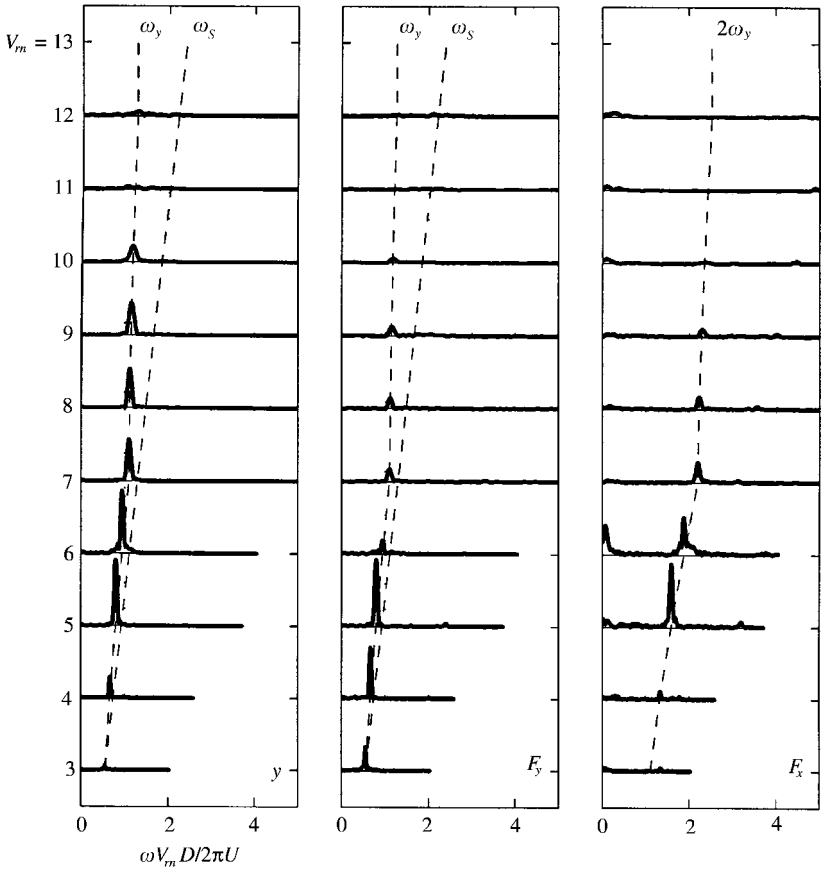

Figure 7. Displacement and force spectra of a single cylinder.

The drag signals present at least four traceable frequency peaks. The dominant force occurs at $2\omega_y$, but there are also harmonics at $3\omega_y$ and $4\omega_y$. Additionally, we see significant energy at $\omega_y + \omega_S$, for $V_{rn} > 11$, above the phase change. Other harmonics may be present as well, although they do not appear to be as repeatable.

When the trailing cylinder is moved to the offset position, the main frequency of motion is still centered just above the structural mode. Lift has a strong component at the shedding rate throughout the range of V_{rn}, although a component at ω_y intensifies at high V_{rn}, as for the in-line case. Drag has a dominant component at ω_y, and a significant second harmonic. We observe fluctuating drag at ω_S and $\omega_y + \omega_S$ also, the latter for the highest range of V_{rn}.

5. DISCUSSION

Both of the wake-interference systems considered show strong galloping, in the sense that vibrations occur for a wide range of reduced velocities, and seem to increase with V_{rn}. The result pertains to a separation distance smaller than that of Brika & Laneville (1999), whose data arguably points to galloping below $S/D = 7$. With regard to the other studies, we employed a much higher Reynolds number than Bokaian & Geoola (1984). High wake sensitivity to Re has in fact been noted for tandem stationary cylinders, but in somewhat

TABLE 1

Physical parameters of some wake-interference VIV studies

Reference	Response	$\mathrm{Re}/10^4$	L/D	Blockage ratio	S_c	m^*
Zdravkovich (1985)*	VR	1–8	11·7	0·042	23	1126
Bokaian & Geoola (1984)†	VR	0·06–0·6	18·1	0·053	1·07	8·42
Brika & Laneville (1999)†	VR, G	0·51–2·75	52·7	0·018	0·78	$\simeq 1000$
Current study†	G	3·2	26·3	0·045	0·95	3·0

* Leading cylinder compliantly mounted. VR: vortex resonance; G: galloping.
† Leading cylinder stationary.

closer proximity (Igarashi 1981). Compliance of the leading cylinder remains a dominant factor in the response; Zdravkovich (1985) observed vortex resonance in the same geometry. Table 1 lists these references, along with some of the physical parameters from the experiments for comparison.

Contrasting with Brika & Laneville (1999), the traceable effect of lower mean velocity on the rear cylinder is not so much an increase in the free-stream V_{rn} at which motion starts, but rather on the location of the phase change. An extrapolation of phase change location from single-cylinder tests can be made using the same mean wake analysis as for the drag coefficient in Section 3 (Huse 1992). In terms of the drag coefficients, the corrected reduced velocity for a feature occurring at V_{rn}^*, in free-stream conditions, is

$$V_{rn}^* \left[\mathrm{mean}(C_d)^{\mathrm{free}}/\mathrm{mean}(C_d)^{\mathrm{wake}}\right]^{1/2},$$

where the superscript "*free*" indicates exposure to the free-stream velocity, and "*wake*" indicates wake flow conditions. Since phase passes through 90° at $V_{rn} \simeq 6{\cdot}5$ for the single cylinder, we then have the estimates $V_{rn} \simeq 10{\cdot}2$ for the in-line wake, and for the offset wake $V_{rn} \simeq 7{\cdot}8$. These values are in good agreement with Figure 4, and suggest that the primary mechanism for V_{rn}-dependent phase change stays remarkably intact in the wake. On the other hand, the trailing cylinders begin to oscillate at the same free-stream V_{rn} as a single cylinder, and at identical frequencies. With respect to a *local* V_{rn} scale, the trailing cylinder locks to the structural mode quite early, by $V_{rn} = 3{\cdot}8$ for the in-line case. Thus, a phase change and frequency locking to the structural mode cannot both define lock-in in the usual sense: wake interference causes these events to occur independently.

Despite the variation of reduced velocity that marks the lift phase change, the component frequencies of lift evolve largely as expected. There are two main peaks at high V_{rn}: ω_S, associated with the stationary leading cylinder, and another $\omega_y \simeq \omega_n$, associated with the primary motion near the structural mode. First, we may observe that no reduction of ω_S is evident; the same value, $\mathrm{St} = 0{\cdot}185$, matches peaks throughout, for every configuration. Thus, the normal shedding mechanism from the leading cylinder is completely unaffected by even the large-scale motions of the trailing cylinder.

With regard to the second component of lift, the drag spectra in the in-line configuration indicate motion-coupled forcing consistent with two or four symmetric vortices per cycle. The existence of a smaller third harmonic of ω_y probably pertains to an odd symmetry such that some forcing cycles may be sporadic. Nonetheless, the typical mechanisms for motion-coupled shedding seem to be present. For the offset case, drag peaks occurring at ω_S correlate with one out of two shed vortices from the leading cylinder reaching the rear cylinder, or at least a significant imbalance in the pressure force from the pair. Note that, in the

corresponding lift spectra, we cannot discern directly whether one or two incoming vortices per cycle cause lift, since they may now act on the same side of the trailing, offset cylinder. The dominant motion-coupled peak in drag near ω_y similarly indicates that the loading has a large asymmetry, especially at high V_{rn}.

6. CONCLUSIONS

Lightly-damped cylinders in free vibrations $4{\cdot}75D$ behind a stationary cylinder are capable of large-scale galloping, helping fill-in a gap between similar tests at larger spacing ratios, and the case of dually compliant cylinders. Frequency lock-in occurs at a low reduced velocity and remains through $V_{rn} = 17$, but the phase change, which typically accompanies frequency lock-in, occurs at higher speeds. This phase change is of the same nature as for single-cylinder tests, and suggests the same fundamental mode transition.

The spectra of the rear cylinder lift and drag forces allow a plausible description of a simple motion-coupled forcing superimposed with a stable wake from the leading cylinder. The former component in the in-line case indicates two or four symmetric vortices per cycle throughout the range of V_{rn}; for the offset cylinder, a one-sided loading is evident. We plan DPIV and anemometry tests to verify these observations.

ACKNOWLEDGEMENTS

We thank Mr F. Gillebo for helping to perform some of the tests and processing. This work is funded by the Office of Naval Research (Ocean Engineering Division), under grant no. N00014-95-1-0106, monitored by Dr T. F. Swean, Jr.

REFERENCES

Bokaian, A. & Geoola, F. 1984 Wake-induced galloping of two interfering circular cylinders. *Journal of Fluid Mechanics* **146,** 383–415.

Brika, D. & Laneville, A. 1993 Vortex-induced vibrations of a long flexible cylinder. *Journal of Fluid Mechanics* **250,** 481–508.

Brika, D. & Laneville, A. 1999 The flow interaction between a stationary cylinder and a downstream flexible cylinder. *Journal of Fluids and Structures* **13,** 579–606.

Hover, F. S., Techet, A. H. & Triantafyllou, M. S. 1998 Forces on oscillating uniform and tapered cylinders in crossflow. *Journal of Fluid Mechanics* **363,** 97–114.

Huse, E. 1992 Current force on individual elements of riser arrays. In *Proceedings second International Offshore and Polar Engineering Conference* (ed. J. Chung). San Francisco: ISOPE.

Igarashi, T. 1981 Characteristics of the flow around two circular cylinders arranged in tandem (First report). *Bulletin of the Japanese Society of Mechanical Engineers* **24,** 323–331.

Mahir, N. & Rockwell, D. 1996 Vortex formation from a forced system of two cylinders. Part 1: tandem arrangement. *Journal of Fluids and Structures* **10,** 473–489.

Williamson, C. H. K. & Roshko, A. 1988 Vortex formation in the wake of an oscillating cylinder. *Journal of Fluids and Structures* **2,** 355–381.

Zdravkovich, M. M. 1985 Flow induced oscillations of two interfering circular cylinders. *Journal of Sound and Vibration* **101,** 511–521.

Zdravkovich, M. M. & Pridden, D. L. 1977 Interference between two circular cylinders; series of unexpected discontinuities. *Journal of Industrial Aerodynamics* **2,** 255–270.